ISBN: 978-3-95450-247-9 ISSN: 2673-5490 doi: 10.18429/JACoW-IPAC2024-THPR30

BEAM OPTICS MODELLING OF SLOW-EXTRACTED VERY HIGH-ENERGY HEAVY IONS FROM THE CERN PROTON SYNCHROTRON FOR RADIATION EFFECTS TESTING *

E. P. Johnson†, A. Bilko, M. Delrieux, L. S. Esposito, N. Emriskova, M. A. Fraser, R. Garcia Alia, P. A. Arrutia Sota, A. Waets, CERN, Geneva, CH

Abstract

Testing of space-bound microelectronics plays a crucial role in ensuring the reliability of electronics exposed to the challenging radiation environment of outer space. This contribution describes the beam optics studies carried out for the run held in November 2023 in the context of the CERN High-Energy Accelerators for Radiation Testing and Shielding (HEARTS) experiment. It also delves into an investigation of the initial conditions at the start of the transfer line from the CERN Proton Synchrotron (PS) to the CERN High Energy Accelerator Mixed-field (CHARM) facility. Comprehensive optics measurement and simulation campaigns were carried out for this purpose and are presented here. Using a validated optics model of the transfer line, the impact of air scattering on the beam size was quantified with MAD-X and FLUKA, providing valuable insights into the current performance and limitations for Single Event Effects (SEE) testing at CHARM.

OPTICS MODEL

CERN High-Energy Accelerators for Radiation Testing and Shielding (HEARTS) [1] use slow-extracted beams from CERN's Proton Synchrotron (PS) to irradiate electronics at the CERN High Energy Accelerator Mixed-field (CHARM) [2] facility. Accurate beam modeling is essential for precisely predicting beam sizes on Devices Under Test (DUTs), ensuring the reliability of radiation effects testing. This section discusses the detailed beam optics measurements undertaken using a lead ion beam with a kinetic energy of $2\,\mathrm{GeV\,u^{-1}}$, aimed at refining the optics model.

Quadrupole Scan Measurement

During Machine Development (MD) studies, quadrupole scans on the PS to East Dump transfer line (F61D) [3] established initial beam conditions post-extraction, capturing the non-linear behavior of the PS main units' edge fields [4–6]. The empirical modeling approach has been shown to be more reliable than a stitched model [7]. The transfer line includes three quadrupoles and a Beam Television (BTV) equipped with a fluorescent screen for beam size measurements. The scans were conducted at the upper energy limits provided by HEARTS to mitigate the impact of beam-material (air, instrumentation, vacuum window) interaction. Py-BOBYQA [8, 9] was chosen as the optimization algorithm to minimize the sum of squared differences between the simulated and measured beam sizes. It was used to determine a set of initial Twiss parameters and normalized emittances, while keeping the dispersion constant. Additionally, kick response measurements validated the beam optics model, giving confidence in the model's representation of the transfer line.

Dispersion Measurement

In a second MD, the dispersion was measured in the T8 transfer line at two different BTV locations (T08.BTV020, T08.BTV035) and at the Multi-Wire Proportional Chamber (MWPC) located at the end of the line (T08.MWPC) [10]. The momentum of the beam was changed by modifying the revolution frequency f_{rev} before extraction (before the RF is turned off and the beam debunched), followed by measuring the centroid movement Δx [11]. Dispersion is given by $D = \Delta x/(\Delta p/p)$, where $\Delta p/p$ is the relative change in the beam's momentum [12]. The change in f_{rev} and the relative change in beam momentum can be expressed as:

$$\frac{\Delta f_{\mathrm{rev}}}{f_{\mathrm{rev}}} = -\eta \frac{\Delta p}{p} \tag{1}$$

where, η is the slip factor, defined as:

$$\eta = \left(\frac{1}{\gamma_{\mathrm{tr}}^2} - \frac{1}{\gamma^2}\right) \tag{2}$$

and $\gamma = 11.41$ is the relativistic Lorentz factor, and $\gamma_{\mathrm{tr}} = 6.13$ is the transition gamma, both determined using a MAD-X [13] model of the PS. The dispersion is calculated from the slopes of the measured changes in centroid position versus the relative change in momentum, corrected by the factor of $\frac{1}{\eta f_{\mathrm{rev}_0}}$ where the initial revolution frequency, f_{rev_0}, is 452.0 kHz and presented in Table 1. A caveat of this measurement is that it was performed for only the nominal quadrupole settings. A more rigorous method would have involved adjusting f_{rev} for each change of optics as the quadrupole strengths were scanned.

Table 1: Dispersion Measurements

Device	D_x	D_y
BTV020	-0.197 ± 0.034	0.035 ± 0.031
BTV035	0.851 ± 0.047	-0.061 ± 0.009
MWPC	-0.963 ± 0.082	-0.169 ± 0.019

* The HEARTS project is funded by the European Union under Grant Agreement No. 101082402, through the Space Work Programme of the European Commission.
† eliott.philippe.johnson@cern.ch

ISBN: 978-3-95450-247-9 ISSN: 2673-5490 doi: 10.18429/JACoW-IPAC2024-THPR30

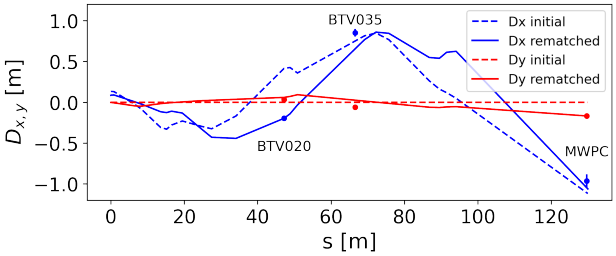

Figure 1: Difference in dispersion before and after the rematch.

A match of the dispersion at the start of the F61 line was done using these measurements, and the optimizer was once again run on the Twiss parameters as they collectively influence the beam size, see Fig. 1. The new set of initial conditions (including the new fixed dispersion) is presented in Table 2.

Table 2: Comparison of Matched Initial Parameters

Parameter	Initial & Re-matched
β_x (m)	53.074 → 66.748
β_y (m)	3.675 → 3.764
α_x	−13.191 → −16.272
α_y	0.859 → 0.703
D_x (m)	0.13 → 0.086
D_y (m)	0.0 → −0.003
D'_x	0.02 → 0.017
D'_y	0.0 → −0.005
ε_{nx} (m^{-5})	2.53 → 2.28
ε_{ny} (m^{-5})	6.94 → 8.63
$\frac{\sigma_E}{E}$	0.0045

AIR SCATTERING

From the PS to the DUT, the beam travels through interceptive instrumentation and air / window regions, during which the emittance increases and the beam energy straggles due to matter interaction [14–17]. Primary effects, such as an increase in beam size, required developing a custom multiple Coulomb scattering module[1] to simulate these changes, compensating for MAD-X's lack of beam-matter interaction modeling, see Fig. 2. The increase in divergence, θ_{rms}, for an ensemble of particles undergoing multiple Coulomb scattering as it passes through a medium is expressed as [18]:

$$\theta_{rms} = \frac{13.6\,\mathrm{MeV\,c^{-1}}}{p\beta_p} q_p \sqrt{\frac{L}{L_{rad}}}$$

where p is the beam's total energy in MeV, q_p the number of charges, L is the length of the interaction and L_{rad} is:

$$L_{\mathrm{rad}} = \frac{L_{\mathrm{rad0}}}{\frac{P_{\mathrm{Torr}}}{760}}$$

where $P = 1.013$ bar is the standard air pressure, and $P_{\mathrm{Torr}} = 750.062 \cdot P$. The radiation length for air, $L_{\mathrm{rad0}} = 301$[2]. The Twiss parameters and emittance evolve from before (0) and after (1) an air region of length L as [19],

$$\begin{aligned}
\alpha_1 &= \frac{\varepsilon_0\alpha_0 - \frac{L}{2}\theta^2_{\mathrm{rms}}}{\varepsilon_0 + \Delta\varepsilon} \\
\beta_1 &= \frac{\varepsilon_0\beta_0 + \frac{L^2}{3}\theta^2_{\mathrm{rms}}}{\varepsilon_0 + \Delta\varepsilon} \\
\varepsilon_1 &= \varepsilon_0 + \frac{1}{2}\theta^2_{\mathrm{rms}}\left(\beta_0 + L\alpha_0 + \frac{L^2}{3}\gamma_0\right)
\end{aligned} \tag{3}$$

The modular design of the code [20] allows for effective handling of multiple Coulomb interactions in any MAD-X sequence. After loading the MAD-X sequence, the user introduces air regions along the sequence with a specified integration length L in meters. The process_scattering() function calculates the impact of the MCS on the beam parameters, generating an updated Twiss output. Upon reaching the "AIR_START" marker, the function records the beta functions using "SAVEBETA" and segments the beam line at this point. It then performs a Twiss calculation with the saved values, updating α, β and ε following Eq. (3). This procedure is repeated at each "INNER_MARKER," refining the beam optics iteratively to account for multiple Coulomb scattering effects in air regions.

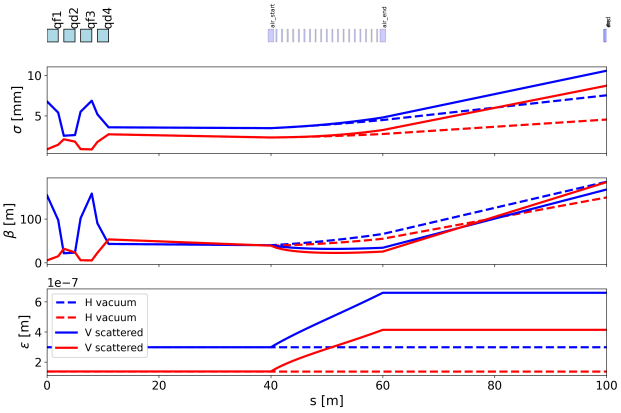

Figure 2: Semi-analytical simulation of multiple Coulomb scattering using a sample lattice.

Semi-analytical results were compared with Monte Carlo simulations that applied random transverse displacements to particle trajectories, simulating scattering with a Gaussian-distributed angle θ_{RMS}. This process emulated the randomness of actual scattering, generating a variety of particle paths to compare statistical beam properties between both methods. Table 3 contrasts these simulation approaches, noting that while the Monte Carlo method requires 30 minutes

[1] An example is available at gitlab.cern.ch/abt-optics-and-code-repository.

[2] cds.cern.ch/record/941314/files/p245.pdf

ISBN: 978-3-95450-247-9 ISSN: 2673-5490 doi: 10.18429/JACoW-IPAC2024-THPR30

for 50,000 particles, the analytical method takes only 1-2 seconds, regardless of the particle count.

Table 3: Simulated beam sizes (in mm) for analytical, Monte Carlo, FLUKA and XSuite methods under non-scattered and scattered conditions using multiple Coulomb interaction only.

σ	Ana.	M.C.	FLUKA	XSuite
H Non-Scat	7.41	7.43	-	-
H Scat	10.50	10.30	10.76	10.05
V Non-Scat	4.53	4.55	-	-
V Scat	8.67	8.45	8.70	8.73

The current HEARTS installation is limited due to extensive air regions along the beam path as it passes through the IRRAD zone to CHARM. One straightforward improvement would be to shift the irradiation from CHARM to IRRAD, which is located just a few meters upstream, minimizing the air seen by the beam before arriving at the DUT.

ENERGY CONTROL

Variation of the ion beam's energy is essential for exploring large parameter space of Linear Energy Transfer (LET) and penetration depth and were developed by CHIMERA at CERN [21–23]. This involves adjusting the magnetic field at the PS's flat top to change beam rigidity. A makerule algorithm recalculates the magnetic field necessary for transfer line magnets. Removing Pole Face Windings (PFW), which are used to control the tune in the PS and do not scale linearly with rigidity [24], ensures smooth energy variations. In 2023, the use of distinct cycles for each energy was replaced by a single cycle managed by a Python script [25] that can be quickly trimmed to seamlessly transition between 650 and 2000 MeV u^{-1} executing changes every 15 –30 s. The cycle also supports energy scans that determine the beam's kinetic energy using penetration tests in materials like Poly-Methyl Methacrylate (PMMA) and speeds up Single Event Effects (SEE) testing of components. Additionally, Python scripting provides control over fluence [26], which is vital for accurate radiation effect testing. A script ensures that the beam is disabled once the target total ion count impacting the DUT is achieved, with fluence measured by the calibrated XSEC070.

Straggling Effects

Energy straggling affects the beam's rigidity as it traverses air regions in F61 and T08. This effect, which was simulated by FLUKA including vacuum windows, air and beam instrumentation [27] was measured by observing the moving transverse position in a dispersive region in the transfer line. As shown in Fig. 3, at T08.BTV35, the lower kinetic energy at extraction leads to a more significant beam displacement, confirming FLUKA's predictions. Installing vacuum chambers, particularly in key areas such as the F61.MBXHD025 switching dipole of F61, is recommended to reduce air-induced straggling. This would optimize VHE ion irradiation at IRRAD/CHARM by improving beam transport.

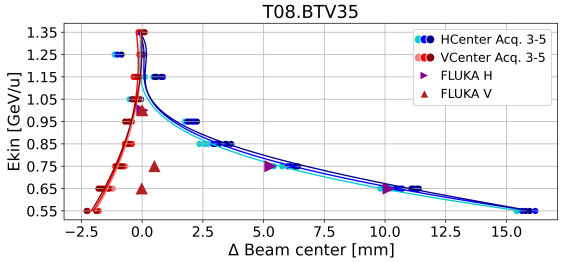

Figure 3: Measurement of the straggling effects in the T8 line at BTV035 compared to FLUKA simulation.

COMPARISON OF MEASUREMENT TO SIMULATION

Figure 4 compares measured and simulated beam sizes at the MWPC, highlighting increased vertical errors due to vacuum pipe aperture interactions distorting the Gaussian shape. These discrepancies occur because the beam isn't centered in the quadrupoles, leading to a varying dipolar moment. Optimized on the shorter East Dump line (27 m) and not the longer T8 line (140 m), the model requires FLUKA validation to address missing interactions like elastic and inelastic air effects and instrumentation influences, particularly at lower energies (600 MeV). Efforts are underway to improve accuracy by adding another MWPC at IRRAD.

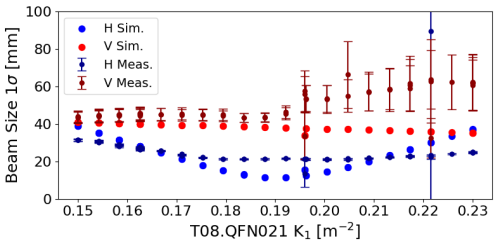

Figure 4: Comparison of beam size measurements and simulation at the MWPC.

CONCLUSION

This study has advanced the beam optics modeling for radiation effects testing with slow-extracted VHE heavy ions from the PS. Key advancements include the refined measurement of initial conditions, the characterization of the dispersion, and the modeling of air scattering through multiple Coulomb scattering. The validated beam model significantly improves the precision and reliability of radiation testing setups. Future improvements will focus on moving HEARTS from CHARM to IRRAD, adding an additional vacuum section to minimize air interactions, and further refine beam control and homogeneity [28]. These contributions not only enhance the robustness of radiation testing at CERN, but also provide valuable insights for similar facilities globally.

ISBN: 978-3-95450-247-9 ISSN: 2673-5490 doi: 10.18429/JACoW-IPAC2024-THPR30

REFERENCES

[1] *HEARTS*, en. https://hearts-project.eu

[2] A. Thornton, *CHARM Facility Test Area Radiation Field Description*, 2016. https://cds.cern.ch/record/2149417

[3] D. Bozzato, J.-F. Gruber, and F. Robert. "Radiation Protection survey during the 2024 commissioning of the new East Dump F6D.TDE018 | Document 3064076 (v.1)." (), https://edms.cern.ch/ui/#!master/navigator/document?D:101495697:101495697:subDocs

[4] J. R. Anglada, "A reference magnetic model of the Proton Synchrotron main units," 2019.

[5] D. Manglunki and M. Martini. "Beam optics modeling at CPS extraction throughout a non-linear fringe field," CERN Document Server. (10, 1997), https://cds.cern.ch/record/324552

[6] T. Zickler, "Influence of shims on the ps main magnets," 1999, SL-Note-99-043 MS. https://cds.cern.ch/record/941314

[7] E. P. Johnson, M. G. Atanasov, Y. Dutheil, M. A. Fraser, and E. Oponowicz, "Beam Optics Modelling Through Fringe Fields During Injection and Extraction at the CERN Proton Synchrotron," in *Proc. IPAC'22*, Bangkok, Thailand, 2022, pp. 511–514. doi:10.18429/JACoW-IPAC2022-MOPOTK030

[8] C. Cartis, L. Roberts, and O. Sheridan-Methven, "Escaping local minima with local derivative-free methods: A numerical investigation," *Optimization*, vol. 71, no. 8, pp. 2343–2373, 2022. doi:10.1080/02331934.2021.1883015

[9] C. Cartis, J. Fiala, B. Marteau, and L. Roberts, "Improving the Flexibility and Robustness of Model-based Derivative-free Optimization Solvers," *ACM Transactions on Mathematical Software*, vol. 45, no. 3, 32:1–32:41, 2019. doi:10.1145/3338517

[10] B. Carlsen *et al.*, "Chapter 4: Beamline – main components," *CERN Yellow Reports: Monographs*, vol. 4, pp. 43–43, 8, 2021. doi:10.23731/CYRM-2021-004.43

[11] M. G. Minty, "Beam Techniques - Beam Control and Manipulation," SLAC National Accelerator Lab., Menlo Park, CA (United States), SLAC-R-621, 24, 2003. doi:10.2172/813024

[12] A. W. Chao, M. Tigner, H. Weise, and F. Zimmermann, *Handbook of Accelerator Physics and Engineering; 3rd Ed.* World Scientific, 2023. doi:10.1142/13229

[13] *MAD - Methodical Accelerator Design*. https://mad.web.cern.ch/mad/

[14] M. Giovannozzi, *Sources of Emittance Growth*, 2005. https://cas.web.cern.ch/sites/default/files/lectures/trieste-2005/giovannozzi-final.pdf

[15] D. E. Groom and S. R. Klein, "Passage of particles through matter," *The European Physical Journal C*, vol. 15, no. 1-4, pp. 163–173, 2000. doi:10.1007/BF02683419

[16] W. Hardt. "A few simple expressions for checking vacuum requirements in a proton synchrotron." (1968), https://cds.cern.ch/record/296859 preprint.

[17] D. Möhl, "Sources of emittance growth," 2006. doi:10.5170/CERN-2006-002.245

[18] A. S. Müller, *Description of Beam-Matter Interaction in the Covariance Matrix Formalism: Application to Modification of Emittance and Twiss Parameters; rev. version*, 2001. https://cds.cern.ch/record/499590

[19] A. S. Müller. "Description of Beam-Matter Interaction in the Covariance Matrix Formalism: Application to Modification of Emittance and Twiss Parameters; rev. version." (2001), https://cds.cern.ch/record/499590 preprint.

[20] "Pybt · master · ABT optics and code repository / Simulation codes / PyBT · GitLab," GitLab. (30, 2023), https://gitlab.cern.ch/abt-optics-and-code-repository/simulation-codes/pybt/-/blob/master/pybt/tools/air_scattering_functions.py

[21] M. A. Fraser *et al.*, "Feasibility of Slow-Extracted High-Energy Ions From the CERN Proton Synchrotron for CHARM," in *Proc. IPAC'22*, Bangkok, Thailand, 2022, pp. 1703–1706. doi:10.18429/JACoW-IPAC2022-WEPOST012

[22] E. P. Johnson *et al.*, "Beam delivery of high-energy ion beams for irradiation experiments at the CERN Proton Synchrotron," in *Proc. IPAC'23*, Venice, Italy, 2023, pp. 315–318. doi:10.18429/JACoW-IPAC2023-MOPA115

[23] A. Waets *et al.*, "Heavy ion beam characterization for radiation effects testing at CERN using Monte Carlo simulations and experimental benchmarking," in *Proc. IPAC'23*, Venice, Italy, 2023, pp. 5165–5168. doi:10.18429/JACoW-IPAC2023-THPM128

[24] A. Asklöv, "Magnetic measurement on the CERN proton synchrotron," LITH-IFM-EX-05/1463-SE, Master's Thesis, Department of Physics and Measurement Technology, 2005.

[25] E. P. Johnson, *Energy GUI Script for CHIMERA*, https://gitlab.cern.ch/eljohnso/chimera_scripts/-/blob/master/energy_GUI.py, 2023.

[26] E. P. Johnson, *Fluence Stop Calculation Script for CHIMERA*, https://gitlab.cern.ch/eljohnso/chimera_scripts/-/blob/master/fluence_stop.py, 2023.

[27] G. Battistoni *et al.*, "Overview of the FLUKA code," *Annals of Nuclear Energy*, vol. 82, pp. 10–18, 2015. doi:10.1016/j.anucene.2014.11.007

[28] W. Scarpa *et al.*, "Investigating transverse noise excitation for improving slow extracted spill quality at the CERN PS," presented at IPAC'24, Nashville, TN, USA, May 2024, paper THPR27, this conference.